Applied Catalysis B: Environmental 251 (2019) 25–36

Contents lists available at ScienceDirect

Applied Catalysis B: Environmental

journal homepage: www.elsevier.com/locate/apcatb

Enhanced electrocatalytic activity of Pd and Pd-polyaniline nanoparticles on electrochemically exfoliated graphite sheets

R. Venkata Jagadeesh, V. Lakshminarayanan*

Raman Research Institute, Bangalore 560080, India

ARTICLE INFO

Keywords:
Flexible graphite sheet
Electrochemical intercalation
Exfoliated graphite sheet
Pd-PANI nanocomposite
Ethanol oxidation reaction

ABSTRACT

The catalyst support materials play an important role in improving the performance of electrocatalysts for alcohol oxidation reaction. In this work, flexible graphite sheets containing a large number of edge planes were electrochemically exfoliated by the application of large positive and negative potentials in acetonitrile medium. The process described here produces several surface functional groups on graphite sheet surface. In this work, the utility of such a functionalized surface is explored as a solid support for depositing Pd and Pd-PANI nanostructures which are studied for oxidation of alcohols in alkaline medium. The results show that these electrode materials exhibit an excellent electrocatalytic activity with very high turnover frequency and low activation energy values for ethanol oxidation reaction that has the potential to be used in low temperature polymer membrane alkaline fuel cells.

1. Introduction

Low temperature fuel cells such as direct alcohol fuel cells (DAFCs) using methanol/ethanol have been emerging as a green technology alternative and is drawing considerable interest worldwide. However, commercialization of these technologies pose significant challenges due to the high cost involved in loading of precious metals for the effective electrocatalytic activity of the device. Researchers have been aiming to optimize the amount of metal to be used without compromising the electrocatalytic activity of the electrode. To address this problem various carbon supports such as graphite, Vulcan XC-72, carbon black, highly oriented pyrolytic graphite, pencil graphite, natural graphite, coke and graphitized silicon supports are used for deposition of noble catalyst materials [1–8].

An inexpensive but effective electrode support material where optimum metal loading can be achieved with large electroactive surface area along with the considerable electrocatalytic activity is an important requirement for DAFCs. The smooth solid supports lack anchoring ability for the metal nanoparticles which might lead to Ostwald ripening eventually. This can create sluggishness for the reactants to diffuse through the electrode which in turn will affect the electrocatalytic activity. In fact, various attempts are being made to improve the electrocatalytic behavior of potential electrocatalysts. Ehrburger et al. have suggested that prior gasification of graphite particles provide a better dispersion of metal nanoparticles. It is due to the surface heterogeneity created on the graphite substrate after pyrolysis step which creates defects on graphite surface. These defects serve as nucleation sites for metal atoms [9]. Xu et al. have suggested that generation of –OH groups on the carbon support enhances the stability of immobilized Pt and Pd nanoparticles [10]. There are well established methods for producing high metal dispersions on carbon, but the resulting substrates are not suitable for the preparation of catalytic material as it involves sintering process for fabrication [11–13]. This issue had motivated numerous studies to improve the metal dispersions on carbon, mainly through optimization of the metal-supporting procedures or functionalization of the carbon surface [14–16].

Flexible graphite is made by compression of stacks of graphite flakes without a binder, where these flakes adhere due to pressure thereby forming a flexible sheet that resembles a piece of thin paper which can be cut easily through scissors. These sheets contain a lot of edges and defects within the surface which in this case serve the purpose of high metal loading. These substrates have the capability of not only to disperse the catalyst particles but also play an important role in enhancing the overall performance. It also offers the advantage of shapability. Conventionally, the flake graphite consists of a lot of edge planes due to which it possess high conductivity [17,18]. A high surface area for the flexible graphite when compared to the other forms of graphite with similar geometric area can be attributed to the presence of large number of edge planes of the graphite flakes. The process also introduces lactone, carboxyl and quinone structure moieties on the edge

* Corresponding author at: Soft Condensed Matter Laboratory, Raman Research Institute, Bangalore 560080, India.
E-mail address: narayan@rri.res.in (V. Lakshminarayanan).

https://doi.org/10.1016/j.apcatb.2019.03.030
Received 23 August 2018; Received in revised form 5 February 2019; Accepted 12 March 2019
Available online 16 March 2019
0926-3373/

surface during the electrochemical treatment [19]. Presence of these functional groups on the surface of exfoliated graphite sheets makes them an excellent substrate for electrochemical deposition of nanomaterials [20]. Zhai et al. and Pieta et al. have synthesized graphitic nitride composite as support for noble metals to obtain effective catalytic oxidation of ethanol, methanol and formic acid [21,22]. Öznülüer et al. observed an enhancement of ethanol oxidation when Cu is under potential deposited onto graphene oxide supports [23].

Researchers have been exploring new routes to enhance the electrocatalytic activity of deposited nanomaterials. This can be achieved by the coating of another reactive metal or metal oxide over the nanomaterial, wiring of nanoparticles within the conducting polymers and functionalizing the support [24,25]. It was earlier shown by us that conducting polymers PANI and PEDOT help in enhancing the electrocatalytic activity of Pd and Au when deposited on gold surface [26,27]. Xu et al. carried out the electrochemical oxidation of methanol and ethanol at Pt and Pd on carbon microspheres (CMS) in alkaline medium. Metal dispersed on CMS shows better electrocatalytic activity compared to the metal dispersed on carbon substrate [10]. Ghosh et al. studied the enhanced electrocatalytic activity of Pd nanoplatelets dispersed on conducting polymers toward ethanol oxidation in alkaline medium [28]. Pandey et al. studied the electrocatalytic behavior of gold dispersed in various conducting polymers like polypyrrole, polyaniline, poly(3,4-ethylenedioxythiophene) and polythiophene toward electrooxidation of ethanol, methanol and formic acid [26].

Herein, we describe the utility of exfoliated graphite sheet as a potential substrate for immobilizing metal nanoparticles. We also show that the Pd-PANI nanocomposite dispersed on the exfoliated graphite electrode shows better electrocatalytic activity compared to just Pd on graphite support. The electrocatalytic activity of these electrodes was studied using cyclic voltammetry and chronoamperometry. The activation energy studies and the effect of surface coverage by reaction intermediates are investigated using Tafel polarization plots. The catalytic efficiency was evaluated using turnover number (TON) and turnover frequency (TOF) obtained from Tafel polarization measurements.

2. Materials and methods

Electrochemical exfoliation of the flexible graphite sheet (GS) was carried out in a classical three electrodes compartment at a constant potential mode. The platinum (Pt) wire was used as counter electrode and silver wire as a reference electrode. Flexible graphite (GS) sheet was used as working electrode for the study. According to the earlier reports, acetonitrile is the preferred solvent for carrying the electrochemical intercalation process [29]. Therefore, the exfoliation process was carried out in acetonitrile using tetrabutyammonium tetrafluoroborate as supporting electrolyte at relatively higher range of positive and negative potentials namely, (±)2.5 V *vs.* silver wire for 300 s [30,31]. Both the processes cause intercalation of the ionic species inside the graphite stacks [32]. The graphite surface exfoliated at positive potential of + 2.5 V is referred to in this work as (+)IGS, while the surface exfoliated at negative potential (− 2.5 V) is referred to as (−) IGS. Exfoliation process occurs through intercalation of ionic species in between the stacks of graphite sheet by increasing the thickness of the electrode [33]. During this process, electrode swelling occurs resulting in some loosely attached fragments detaching from the surface due to intense gas evolution. A contraction across the width of the electrode happens after the removal of electrode from solution which can be attributed to the restacking of the graphite layers [34]. This integral electrode was quite stable and possesses structural integrity that could be used for immobilization of metal nanostructures.

2.1. Electrochemical exfoliation of graphite sheets

Electrochemical exfoliation of the flexible graphite sheet (GS) was carried out in a three electrode compartment at a constant potential mode. The platinum (Pt) wire was used as counter electrode and silver wire as a reference electrode. Flexible graphite (GS) sheet was used as working electrode for the study. According to the earlier reports, acetonitrile is the preferred solvent for carrying the electrochemical intercalation process [29]. Therefore, the exfoliation process was carried out in acetonitrile with tetrabutylammonium tetrafluoroborate (TBATFB) as a supporting electrolyte at relatively higher range of positive and negative potentials namely, (±)2.5 V *vs.* silver wire for 300 s [30,31]. Both the processes cause intercalation of the ionic species inside the graphite stacks [32]. The graphite surface exfoliated at positive potential of + 2.5 V is referred in this work as (+)IGS, while the surface exfoliated at negative potential (− 2.5 V) is referred as (−)IGS. Exfoliation process occurs through intercalation of ionic species in between the stacks of graphite sheet by increasing the thickness of the electrode [33]. During this process, electrode swelling occurs resulting in some loosely attached fragments detaching from the surface due to intense gas evolution. A contraction across the width of the electrode happens after the removal of electrode from solution which can be attributed to the restacking of the graphite layers [34]. This integral electrode was quite stable and possesses structural integrity that could be used for immobilization of metal nanostructures.

2.2. Preparation of Pd-PANI nanocomposite

Pd nanoparticles are produced by electrochemical process from the electrolytic solution of 1 mM $PdCl_2$ in 0.5 M HCl. Graphite rod of diameter 4 mm is used as working electrode and flexible graphite sheet (GS) or electrochemically exfoliated graphite sheets ((±)IGS) are used as counter electrodes for the deposition of Pd nanoparticle and Pd-PANI nanocomposites. Pd nanoparticles are deposited by the application of 10 mA/cm^2 current density in 1 mM $PdCl_2$ solution, whereas deposition of Pd-PANI is carried out by dissolution of 5 µL aniline + 1 mM $PdCl_2$ + 0.1 M HCl solution by the application of 10 mA/cm^2 current density corresponding to graphite rod respectively. The dissolved palladium ions form hexachloropalladate complex in the acid solution. Highly oxidizing tendency of this palladium complex initiates the polymerization of aniline which in turn gets reduced to palladium metal atoms. The reduced Pd metal atoms cluster together and adhere to the PANI film resulting in the Pd-PANI nanocomposite [7]. Pd-PANI nanocomposite is positively charged due to the protonation in acid electrolyte, which electrophoretically deposit onto the electrode substrate as a thin film.

Deposition of Pd-PANI nanocomposite was carried out by chronopotentiometry technique by applying a 10 mA/cm^2 current density with respect to the anode. This value of current density was chosen for the deposition, as it provides an integral electrode even after exfoliation while possessing good mechanical stability. We have carried out the deposition in galvanostatic mode for 1000 s with different current values to study the effect of current on the nature of coating. A schematic representation of polymerization of aniline in the presence of palladium is shown in Fig. S1 (supplementary material) [35].

3. Results and discussion

The electrochemical techniques used for the studies are chronoamperometry (CA), chronopotentiometry (CP), cyclic voltammetry (CV). The characterization of the materials were carried out using Raman spectroscopy, X-ray diffraction (XRD), atomic force microscopy (AFM), scanning electron microscopy (SEM), energy dispersive spectroscopy (EDAX), scanning transmission electron microscopy (STEM) and scanning tunneling microscopy (STM) techniques.

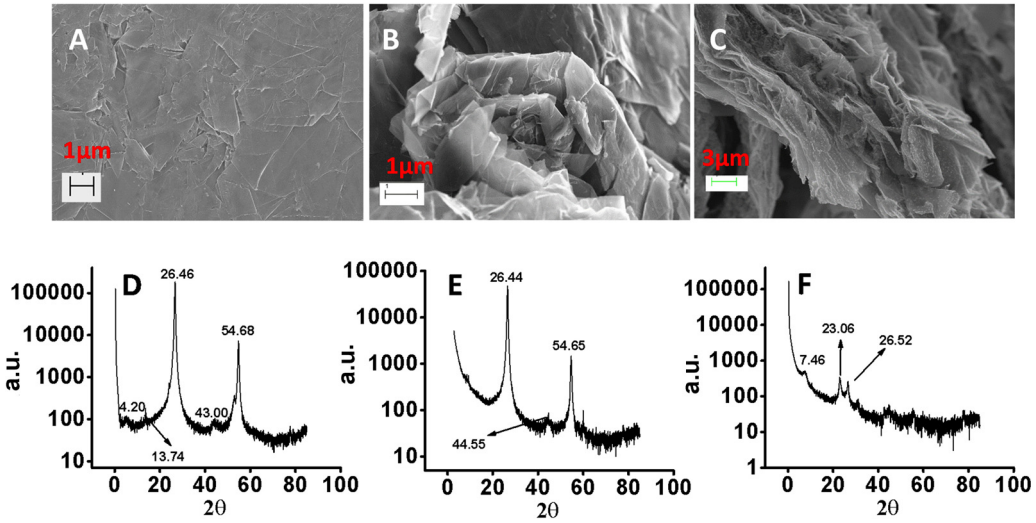

Fig. 1. SEM images and XRD plots of (A, D) GS, (B, E) (+)IGS and (C, F) (−)IGS substrates.

3.1. SEM and XRD analysis of flexible graphite and exfoliated graphite sheet

The morphologies of the flexible graphite sheet (Fig. 1A) and the electrochemically exfoliated graphite substrates (Fig. 1B and C) are examined using SEM. As shown in Fig. 1A, the surface of the graphite sheet reveals a flaky structure with graphite sheets of varying sizes stacked together along their basal planes [4]. It also consists of highly-oriented graphite layers which are very thin with varying sizes in the micrometer (μm) range [38]. It is also observed that a few gaps are present on the surface which means these bundles are not stacking uniformly. On the contrary, Fig. 1B and C shows the images after exfoliation which comprise of wrinkled or folded thin sheets. This is due to the intercalation of ions in between graphite layers which reduces the planarity of basal planes thereby revealing a large amount of edge planes of graphite substrate. The surface roughness increases due to the formation of folds and corrugations on graphite substrates after electrochemical exfoliation. AFM and STM characterization studies of flexible graphite sheet are shown in Fig. S2 in the supplementary information. The images show that the surface after exfoliation possesses layered structure consisting of graphite flakes which are bonded together while the individual flakes exhibit atomically smooth features with typical hexagonal lattice.

Fig. 1D–F shows XRD plots of GS, (+)IGS and (−)IGS substrates respectively. Fig. 1D shows two prominent sharp peaks around positions (2θ) 26.5° (002) and 54.6° (004) respectively which reflect the order and polycrystallinity of the substrate [39]. The peaks around 26.5° and 54.6° are retained even after electrochemical intercalation. The sharp and highly intense (002) peak in Fig. 1D shows that GS is highly ordered. However, after exfoliation there is a decrease of peak intensity. This is due to the decrease in the thickness of the GS along the stacking direction of basal planes of graphite during intercalation process. The sharp peaks in all the cases indicate that the crystallinity of the substrate is still retained even after exfoliation of graphite sheet [6].

By using Bragg's equation $n\lambda = 2d \sin\theta$, the interlayer distances of the substrates were measured, where n is a positive integer, λ is the wavelength of incident wave, d is the interplanar distance and θ is the angle of incidence.

The values obtained for GS, (+)IGS and (−)IGS are 0.337, 0.338 and 0.338 nm respectively. The values of interlayer spacing in exfoliated graphite sheets show very small increase when compared to that of the graphite sheet due to the restacking of graphite layers after exfoliation.

The Raman characterization results of GS and (±)IGS were shown in Fig. S3 of supplementary information. They show that there is a significant increase in I_D/I_G ratio suggesting that the exfoliation process creates a large number of defects in the graphite surface. The (+)IGS substrate shows considerably more defects which can be attributed to the formation of several oxygen containing functional groups such as carboxyl, hydroxyl and epoxide *etc.*, created on the surface due to surface oxidation of graphite [36,37].

Table 1 shows Raman shift values for GS, (+)IGS and (−)IGS samples where I_D/I_G ratio is also shown. It is known that ratio of I_D/I_G reflects the surface defect density of graphite. It can be seen that the (+)IGS shows largest I_D/I_G ratio implying the presence of large number of defects. However, in the negative potential exfoliated graphite (−)IGS the surface defects have increased when compared to the graphite substrate. However, it is very much less than that of positive exfoliated graphite. This is because of the fact that the surface oxidation at positive potentials introduces several functional groups causing large number of defect sites when compared to the negatively exfoliated surface.

3.2. Morphological characterization of Pd/GS, Pd-PANI/GS, Pd-PANI/(+)IGS and Pd-PANI/(−)IGS substrates

Fig. 2 shows the high resolution SEM images and corresponding surface elemental analysis measured by EDAX for (A) Pd/GS, (B) Pd-PANI/GS, (C) Pd-PANI/(+)IGS and (D) Pd-PANI/(−)IGS respectively. It can be seen that the Pd nanoparticles on graphite sheet have formed as clusters of 100–200 nm which in turn are aggregated as domains (Fig. 2A). The Pd-PANI nanocomposite deposited on the graphite surface form nanoclusters which show cauliflower shaped domains (Fig. 2B). Fig. 2C and D shows Pd-PANI deposited on (+)IGS and (−)IGS substrates exhibiting globular structures and cylindrical rod like features respectively. These images suggest a diffusion controlled aggregation growth [40] during electrodeposition. The corresponding energy dispersive X-ray (EDAX) plots show that these substrates are

Table 1
Raman shift values obtained for GS and electrochemically intercalated graphite sheets (±)IGS at +2.5 V and −2.5 V using 0.1 M TBATFB in acetonitrile solvent.

Substrate	D band (cm^{-1})	G band (cm^{-1})	2D band (cm^{-1})	I_D/I_G
GS	1325	1571	2667	0.20
(+)IGS	1328	1591	2635	1.69
(−)IGS	1325	1572	2635	0.53

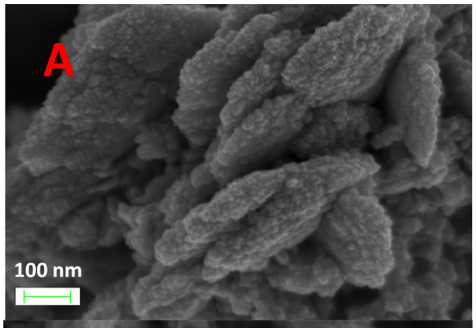

Element	Weight%
C	2.27
Pd	97.73
Total	100

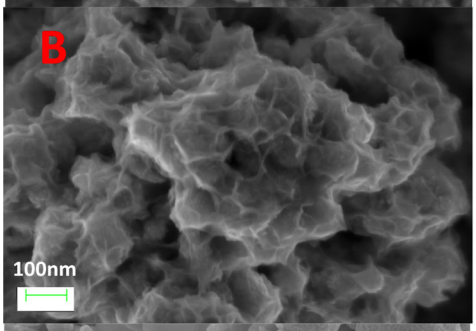

Element	Weight%
C	8.51
N	2.37
Pd	89.12
Total	100

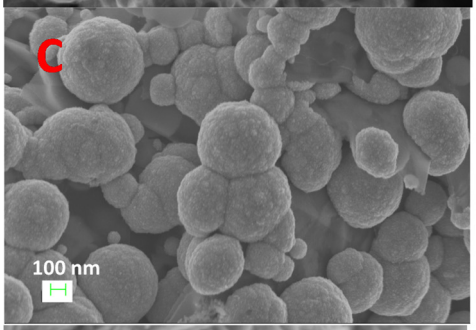

Element	Weight%
C	20.15
N	6.05
O	2.56
Pd	71.24
Total	100

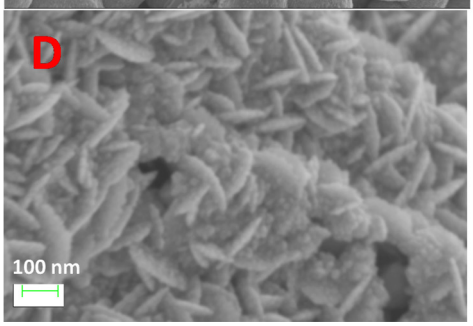

Element	Weight%
C	23.04
N	6.36
O	2.02
Pd	68.58
Total	100

Fig. 2. Scanning electron micrographs images of (A) Pd/GS, (B) Pd-PANI/GS, (C) Pd-PANI/(+)IGS and (D) Pd-PANI/(−)IGS substrates. *Note*: Elemental analysis by EDAX are given next to the respective substrate (average of the values measured of four different regions).

mainly composed of Pd (Fig. S4). The peaks corresponding to C, N and O elements are from the polymer matrix as well as from the oxygen functionalities formed on the surface during the electrochemical exfoliation.

Fig. 3 shows the STEM images of (A) Pd/GS, (B) Pd-PANI/GS, (C) Pd-PANI/(+)IGS and (D) Pd-PANI/(−)IGS substrates. Fig. 3A shows the image of Pd/GS which are actually polyhedral nanoclusters of sizes ranging from 150 to 200 nm (see Fig. S5A in supplementary information). The formation of these clusters suggest that these are aggregation of Pd nanoparticles which have similar features as in the SEM image of Fig. 2A. Fig. 3B and C shows several nanostructures in addition to smaller nanoparticles which together form the film on the surface. The surface of Pd-PANI/(−)IGS shows Pd nanoparticles are enclosed within the sharp edged domains of PANI (Fig. 3D). The supplementary information (Fig. S5) shows the STEM images of the respective samples in closer ranges.

3.3. XRD studies of Pd-PANI/GS, Pd-PANI/(+)IGS and Pd-PANI/(−)IGS

Fig. 4 shows the X-ray diffraction pattern of Pd-PANI nanocomposite deposited on (A) GS, (B) (+)IGS and (C) (−)IGS substrates respectively. The sharp peak patterns indicate the highly crystalline features of the deposit. The Pd-PANI deposited on all the three substrates show respective peaks at 40.13° (111), 46.90° (200), 68.30° (220) and 82.50° (311) angles which can be indexed to fcc nanostructure [41]. The additional sharp peaks are due to the respective substrate on which the nanocomposite was deposited. The crystallite size (D) can be calculated using Debye–Scherrer equation:

$$D = \frac{k\lambda}{\beta \cos\theta}$$

k is a dimensionless shape factor (0.94) with a value close to unity, λ is the X-ray wavelength, β is the line broadening at half the maximum intensity (FWHM) (radians) and θ is the Bragg angle. The calculated

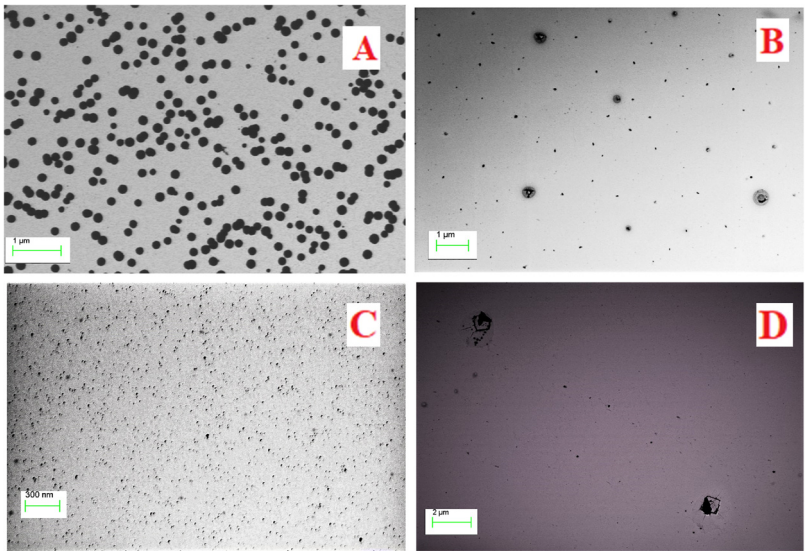

Fig. 3. Scanning transmission electron microscopy images of (A) Pd/GS, (B) Pd-PANI/GS, (C) Pd-PANI/(+)/IGS and (D) Pd-PANI/(−)IGS substrates.

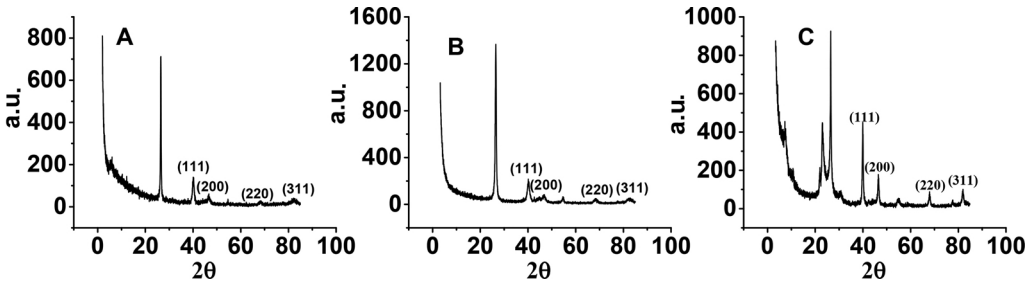

Fig. 4. X-ray diffraction graphs of Pd-PANI nanocomposites deposited on (A) GS, (B) (+)IGS and (C) (−)IGS substrate respectively.

Table 2
Crystallite sizes of Pd-PANI nanocomposite deposited on GS, (+)IGS and (−)IGS substrates.

Peak position (2θ)	Crystallite size (nm)		
	Pd-PANI/GS	Pd-PANI/(+)IGS	Pd-PANI/(−)IGS
40.1	8.5	7.3	4.7
46.9	7.3	8.1	17.2
68.3	8.8	5.2	14.4
82.5	6.3	3.5	9.6

crystallite size values for the deposited composite are shown in Table 2. It can be seen that Pd crystallite sizes vary with the nature of the substrate.

3.4. Cyclic voltammetric studies on exfoliated graphite

Fig. 5 shows the voltammetric behavior of the (A). Pd-PANI/GS, (B). Pd-PANI/(+)IGS and (C). Pd-PANI/(−)IGS electrode in 0.5 M H_2SO_4 at a scan rate of 100 mV/s. The voltammograms show two prominent redox peaks which were common in all the cases. The peak around −0.2 V *vs.* MMO during the anodic scan corresponds to the oxidation of adsorbed hydrogen and another peak around +0.4 V during the cathodic scan is due to the reduction of PdO which is formed during the forward positive potential scan [26,42]. Since Pd has the ability to adsorb as well as absorb H_2 onto it, the area measured by calculating the charge under the peak I does not reflect the true surface area of the Pd in the nanocomposite [43]. Nevertheless, the electrocatalytic surface area (ECSA) of Pd can be calculated from the PdO stripping peak [43,44]. The charge values measured by the integration of PdO stripping peak are 28, 87.8 and 97.5 mC for Pd-PANI nanocomposite electrodes deposited onto GS, (+)IGS and (−)IGS substrates respectively which translate into true ECSA of 66, 207 and 230 cm^2 respectively. Exfoliation of the graphite sheet results an increase in the loading of palladium which can be attributed to the increase of surface sites for deposition of Pd-PANI nanocomposite. It is worth noting that overall increase in true surface area of Pd is almost the same during the positive and negative exfoliation processes. The background currents of the graphite sheet electrode increase by from 0.6 mA to 2.4 mA (+IGS) and 3 mA (−IGS) after exfoliation step.

3.4.1. Mechanism of electrocatalytic oxidation of ethanol

Ethanol oxidation in alkaline media has been studied extensively by various groups due to its potential applications in alkaline fuel cells [24,25,45]. Eqs. (1)–(4) show the steps followed during the reaction. The process involves the adsorption of reactants and intermediates through the hydroxyl group on the electrode surface [46,47]. The reaction takes place through three intermediate steps by the formation of acetaldehyde and acetic acid as the intermediates and carbon dioxide as the final product [26,48]. The complete oxidation of ethanol to CO_2 is inhibited because of the adsorption on the electrode surface by the reaction intermediates which poison the surface sites thereby bringing down the electrocatalytic activity of the nanomaterial with time.

$$3C_2H_5OH + 3OH^- \rightarrow 3CH_3CO_{ads} + 3H_2O \quad (1)$$

$$OH^- \rightarrow OH_{ads} \quad (2)$$

$$CH_3CO_{ads} + OH_{ads} \rightarrow CH_3COOH \quad (3)$$

$$CH_3COOH + OH^- \rightarrow CH_3COO^- + H_2O \quad (4)$$

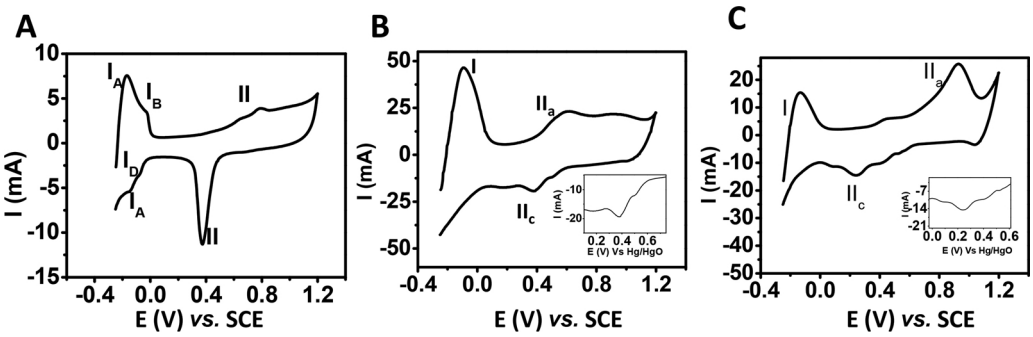

Fig. 5. Cyclic voltammograms of (A) Pd-PANI/GS (C_{dl} = 23 mF), (B) Pd-PANI/(+)IGS (C_{dl} = 233 mF) and (C) Pd-PANI/(−)IGS (C_{dl} = 133 mF) in 0.5 M H_2SO_4 solution.

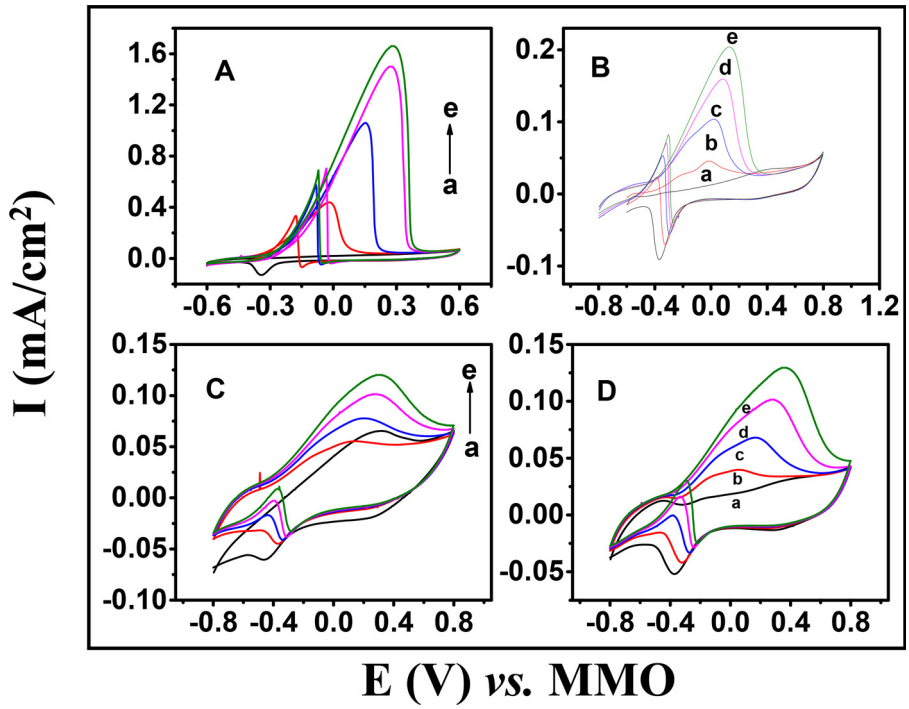

Fig. 6. Cyclic voltammograms of (A) Pd/GS (0.1–0.4 M ethanol), (B) Pd-PANI/GS (0.05–0.2 M ethanol), (C) Pd-PANI/(+)IGS (0.01–0.04 M ethanol) and (D) Pd-PANI/(−)IGS (0.01–0.04 M ethanol) electrode at various ethanol concentrations using 0.1 M NaOH *vs.* MMO reference electrode.

3.4.2. CV studies for ethanol oxidation reaction (EOR)

Fig. 6 shows CV of (A) Pd/GS, (B) Pd-PANI/GS, (C) Pd-PANI/(+)IGS and (D) Pd-PANI/(−)IGS electrodes at various ethanol concentrations using 0.1 M NaOH at a scan rate of 50 mV/s. An oxide stripping reduction peak of PdO to Pd around −350 mV *vs.* MMO can be seen in all the cases. The CVs also show the effect of varying ethanol concentrations. The peak currents due to the oxidation of ethanol during the forward scan is normally used to analyze the catalytic activity of an active material [49]. From Fig. 6, it can be seen that the peak potential in the anodic scan shift toward positive direction with the increase in concentration of ethanol. The positive shift in peak potential can be attributed to the increase in coverage by reactant molecules on Pd sites at higher ethanol concentrations [50]. According to the previous reports, adsorbed hydroxyl ions play a key role in enhancing the electrocatalytic activity of the electrode [46]. The concentration of ethanol has been optimized to 0.4 M for the studies on Pd/GS, 0.2 M for Pd-PANI/GS and 0.04 M for Pd-PANI/(+)IGS and Pd-PANI/(−)IGS electrodes. The cyclic voltammograms show a typical ethanol oxidation peak during the anodic scan while the reverse positive current peak during the cathodic cycle is associated with the oxidation of intermediate species adsorbed on Pd surface [46]. The ethanol oxidation currents on the surface of Pd-PANI/GS show higher currents even at an ethanol concentration as low as 40 mM in contrast to similar currents at 0.2 M ethanol for Pd/GS. This behavior demonstrates that the highly porous and hierarchical pore structure of electrodeposited Pd electrode causes an enhanced ethanol oxidation reaction. Remarkably, the reverse anodic peak currents are lower in the case of Pd-PANI/GS electrode compared to Pd/GS which suggests that concentration of adsorbed intermediates on Pd-PANI is very much less, even though the forward oxidation current is more in the case of the latter. The significant increase in the ethanol oxidation currents on Pd-PANI surface and lesser surface adsorbed intermediate species on it confirm the better electrocatalytic activity of Pd-PANI/GS compared to Pd/GS substrate.

3.4.3. Long term stability tests

Fig. 7 shows the long term stability CV curves for the EOR on (A) Pd/GS, (B) Pd-PANI/GS, (C) Pd-PANI/(+)IGS and (D) Pd-PANI/(−)IGS electrodes (Fig. 7). For this, we have conducted the CV for 1000 cycles (approx. 12 h). We observe that the EOR current decrease gradually when scanned up to 1000 cycles (Fig. S6). This decrease arises due to some reaction intermediates getting trapped with graphite oxide layers

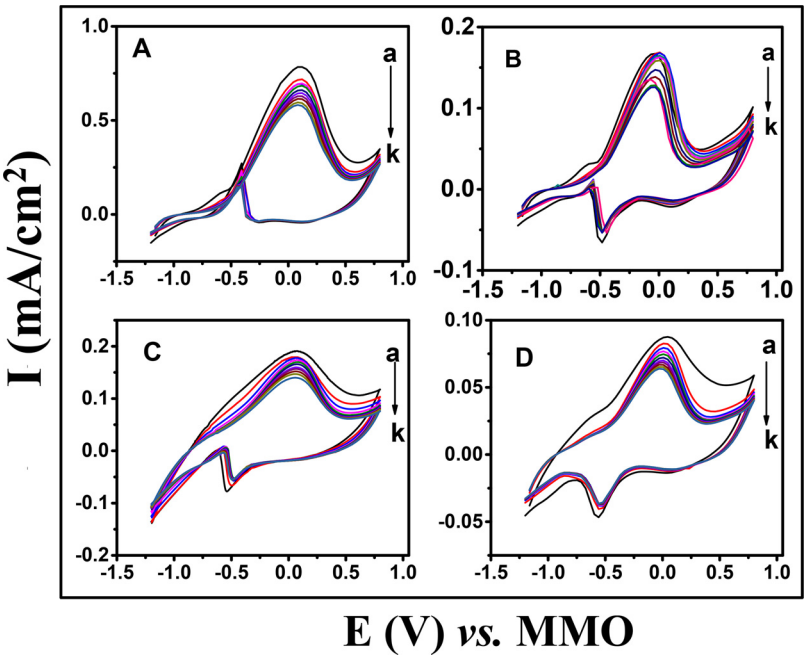

Fig. 7. (a) 1st, (b) 100th, (c) 200th, (d) 300th, (e) 400th, (f) 500th, (g) 600th, (h) 700th, (i) 800th, (j) 900th and (k) 1000th cycle CV curves for (A) Pd/GS (0.1 M), (B) Pd-PANI/GS, (0.05 M) (C) Pd-PANI/(+)IGS (0.01 M) and (D) Pd-PANI/(−)IGS (0.01 M) ethanol oxidation reaction in 0.1 M NaOH solution at a scan rate of 100 mV/s.

and blocking the active sites. However, the stability results show that electrooxidation current remains stable till about 500 cycles for Pd-PANI/GS substrate, when compared to the Pd/GS electrode, which suggests that the substrate stability is increased after modifying with the PANI film. The current responses for EOR on Pd/GS, Pd-PANI/GS, Pd-PANI/(+)IGS and Pd-PANI/(−)IGS at various cycle numbers are shown in Fig. S6 (supporting information). This study shows that the electrocatalytic activity of electrodeposited Pd-PANI on GS and (±) IGS is stable during continuous cycling for 12 h with moderate decrease in the efficiency of the catalytic surface.

Having attained the stability information of the Pd/GS, Pd-PANI/GS, Pd-PANI/(+)IGS and Pd-PANI/(−)IGS substrates by CV, it is worthwhile to investigate using the chronoamperometry study to find out the nature of steady state current for EOR. Fig. S7 shows the chronoamperometry curves in EOR on electrodeposited Pd/GS and Pd-PANI/GS or (±)IGS substrates measured at the peak potential in the CV of ethanol oxidation for the respective electrode (Fig. 6). It is seen that the current decreases initially and reaches a steady state within about 100 s and remains at the steady state for the entire duration of the experiment.

3.4.4. Reaction kinetics study of EOR

The reaction kinetics of the EOR can be studied by measuring the effect of ethanol concentration on the reaction rate and calculating the reaction order by plotting the $\log I$ *vs.* $\log C$ (ethanol concentration) as shown in Fig. S7 [26]. The reaction order was calculated by using the following equation [51]:

$$I = nFkc^m$$

which can be expressed as

$$\log I = \log nFk + m \log c$$

where F – Faraday constant, k – reaction constant, c – ethanol concentration and m – reaction order with respect to ethanol.

The slope of the graph at a given potential provides the apparent reaction order (m) of ethanol electrooxidation reaction with respect to the ethanol concentration. The order of the reaction was calculated at two different potentials namely, −0.4 and −0.1 V *vs.* MMO reference electrode. The values of the measured reaction orders for Pd/GS, Pd-PANI/GS, Pd-PANI/(+)IGS and Pd-PANI/(−)IGS electrodes are shown in Table S1 from which it can be concluded that the reaction mechanism exhibits significant change in the reaction order with potentials in all the cases except on Pd-PANI/(+)IGS. This leads to the inference that the reaction kinetics is influenced significantly by the applied potential in the case of the three systems which can be attributed to the availability of the active sites for adsorption of the molecules at a more positive potential of −0.1 V when compared to that at −0.4 V.

3.4.5. Tafel analysis of EOR

Tafel plots (over potential (η) *vs.* $\log I$) provide useful information which can help in understanding the nature and mechanism of the alcohol oxidation reactions in addition to the extent of surface coverage by the intermediates during the electrochemical process. These plots do not often follow the Butler–Volmer equation in the case of reactions where the surfaces are covered with intermediates during catalytic process [46]. Therefore, the measured Tafel slopes deviate drastically from ideal values and are higher than the usual electron transfer processes on pristine surfaces. This is due to the fact that the adsorbed reactive intermediates formed on the catalytic surface decrease the available active sites for the fresh reactant molecules to adsorb thereby bringing down the currents. This is reflected as increased Tafel slopes in polarization plots. It must be noted that the current density calculated for the measurement of Tafel slopes is with respect the electrochemically active surface area (ECSA). The ethanol oxidation on Pd surface occurs through dissociative chemisorption of ethanol to form acetic acid and acetaldehyde, the active intermediate formed during the reaction which adsorbs strongly on the electrode surface [46,52]. Since the adsorption of reactive intermediates is a dynamic process which vary with overpotential, the measured Tafel slopes reflect the extent of availability of active sites during the reaction.

The steps involved in ethanol oxidation reaction have been shown in Eqs. (1)–(4). The removal of CH_3CO_{ads} radical by adsorbed hydroxyl group (Eq. (3)) is the rate determining step of the reaction [10]. Recently, Ma et al. carried out a comparative study of the ethanol electrooxidation on Pt/C and Pd/C surfaces in alkaline medium and observed that Pd/C shows higher catalytic activity in alkaline medium [53]. Tripković et al. have suggested that the electrooxidation of ethanol at palladium surface follows a dual-path mechanism where acetic acid is the final product in one and carbon dioxide in the other pathway. They also suggested that acetic acid is the major product

Table 3
Tafel slopes (mV/dec) for EOR process at Pd/GS, Pd-PANI/GS, Pd-PANI/(+)IGS and Pd-PANI/(−)IGS electrodes respectively.

T (K)	Pd/GS		Pd-PANI/GS		Pd-PANI/(+)IGS		Pd-PANI/(−)IGS	
	Slope 1	Slope 2	Slope 1	Slope 2	Slope 1	Slope 2	Slope 1	Slope 2
288	270.7	674.6	211.7	386.9	193.1	512.7	219.4	490.3
293	222.6	590.8	164.7	341.5	216.5	592.4	221.7	481.7
298	174.7	582.1	136.1	375.5	184.8	572.7	208.6	478.8
303	163.8	635.5	125.4	447.2	171.6	275.2	194.3	594.2
308	178.8	635.5	114.7	405.2	184.9	636.7	187.1	445.4

when catalyzed by the adsorbed hydroxyl groups on the surface [52]. Wang et al. studied the electrooxidation of ethanol on Pt/C electrode at various concentrations of ethanol and observed that at low concentrations (1 mM), acetic acid is the main product while at higher concentrations (0.5 M) it is acetaldehyde [54].

Table 3 shows the Tafel slopes measured from the Tafel polarization plots (supplementary Figs. S8 and S9) on Pd/GS and Pd-PANI/GS electrodes in 0.2 M ethanol, Pd-PANI/(+)IGS and Pd-PANI/(−)IGS in 0.04 M ethanol using 0.1 M NaOH supporting electrolyte at various temperatures. These measurements were carried out at a temperature range of 15–35 °C and in the potential range of −400 to −50 mV *vs.* MMO reference electrode. The concentration of ethanol used for catalytic studies was based on the prior CV measurements of the samples in the respective systems. These plots show abnormally high values of Tafel slopes compared to 120 mV expected for a typical one electron process, which can be explained by the adsorption of the carbonaceous intermediates resulting in the surface poisoning. This diminishes the active reaction sites for the fresh ethanol molecules thereby causing a decrease in current [46,55]. Therefore, a study of Tafel polarization plots provide wider perspective about the reaction process. Further, the change in the Tafel slope values with temperature is an indicator of the extent of adsorption of the reaction intermediates which inhibits the reactant molecules from adsorbing on the Pd/GS and Pd-PANI/GS electrode as the reaction advances. It can be seen that, there is a decrease of the Tafel slope values with increasing temperature. Lower Tafel slopes at higher temperatures indicate higher oxidation current at any given overpotential. Since the desorption of reaction intermediates is more facile at higher temperatures, the surface coverage decreases at higher temperatures.

Sai Siddhardha et al. studied the ethanol oxidation on gold nanocomposites and observed two Tafel slopes for oxidation reaction [55]. Similarly, the data obtained in the present study exhibit two distinct slopes, with the value of second slope being higher than the first. Since the measured current at each overpotential is dependent on the availability of the free surface sites on the electrode, it is possible to correlate the change in the Tafel slope with the extent of surface poisoning during the course of the reaction. In our study, there is a distinct decrease in the first Tafel slope values with increase in temperature (Table 2), which points to an increase in the ethanol oxidation currents with increasing temperatures. This effect is due to the decline in the surface passivation with increasing temperature on the Pd-PANI nanocomposite electrode surface leading to an overall enhancement of electrocatalytic activity of the nanocomposite system at higher temperatures.

3.4.6. Turnover number (TON) and turnover frequency (TOF) calculation from chronoamperometry studies

The turnover number (TON) and turnover frequency (TOF) values are useful parameters to evaluate the catalytic efficiency of the nanocomposites which have been calculated in this work from the chronoamperometric measurements at different potentials.

Turnover number (TON) is a sign of the number of alcohol molecules oxidized per unit surface area per second, which reveals the current in steady state for electrooxidation process. It was calculated using the equation below:

$$\text{Turnover number (TON)} = \frac{I \times N_A}{n \times F \times m_{Pd}} \quad (5)$$

where I = current density (mA cm^{-2} mol^{-1}), N_A = Avogadro number, F = Faraday constant (A s/mol) and m_{Pd} = mean atomic density of surface ($m_{Pd} = 1.0 \times 10^{15}$ atoms number cm^{-2})

Turnover frequency (TOF) quantifies the number of alcohol monolayers that are electrooxidated per unit time and it is calculated using the equation

$$\text{Turnover frequency (TOF)} = \frac{\text{TON}}{t} \quad \{t = 10\,\text{s}\} \quad (6)$$

Fig. 8 shows the TON and TOF *vs.* temperature curves of ethanol oxidation at 0 V *vs.* MMO on (A) Pd/GS, (B) Pd-PANI/GS, (C) Pd-PANI/(+)IGS and (D) Pd-PANI/(−)IGS electrodes respectively. Table 4 shows the TON and TOF values obtained from the analysis of the results. Higher values of TON and TOF imply better catalytic efficiency as more molecules are oxidized per unit area per second. It can be seen from Table 4, that TON and TOF values of Pd-PANI deposited on exfoliated graphite sheets show higher efficiency when compared to Pd/GS and Pd-PANI/GS. The enhanced efficiency can be attributed to more surface functional groups on GS which bind effectively with Pd nanoparticle and Pd-PANI nanocomposite. The TON and TOF values reported here for the ethanol electrooxidation in alkaline medium are more than two orders of magnitude higher compared to the value reported by Kaedi et al. for Pd-PNMSS in alkaline medium [56].

The TON and TOF values obtained for ethanol oxidation at the Pd-PANI nanocomposite at various overpotentials on various substrates under study are shown in supporting information (Tables S2–S5).

It was earlier reported that the formation of oxygen functional groups on supporting graphite substrate increases the catalytic activity of Pd-based catalysts toward alcohol oxidation [10,57,58]. The hydrophilic surface functional groups provide easy access to the alcohol molecules to diffuse through the pores and channels that significantly

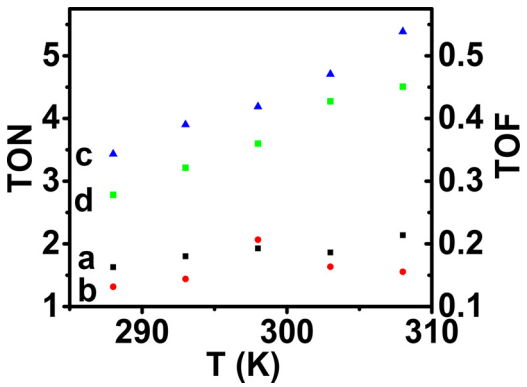

Fig. 8. Turnover number (TON) and turnover frequency (TOF) values calculated at 0 V *vs.* MMO for ethanol oxidation on (a) Pd/GS (0.4 M), (b) Pd-PANI/GS (0.2 M), (c) Pd-PANI/(+)IGS (0.04 M) and (d) Pd-PANI/(−)IGS (0.04 M) using 0.1 M NaOH electrolyte.

Table 4
Turnover number (TON) and turnover frequency (TOF) values for ethanol electrooxidation on Pd/GS, Pd-PANI/GS, Pd-PANI/(+)IGS and Pd-PANI/(−)IGS substrates at 0 V *vs.* MMO reference electrode.

Substrate	Turnover Number (TON) (s^{-1})					Turnover Frequency (TOF)				
	288 K	293 K	298 K	303 K	308 K	288 K	293 K	298 K	303 K	308 K
Pd/GS	1.6	1.8	1.9	1.8	2.1	0.16	0.18	0.19	0.18	0.21
Pd-PANI/GS	1.3	1.4	2.1	1.6	1.6	0.13	0.14	0.21	0.16	0.16
Pd-PANI/(+)IGS	3.4	3.9	4.3	4.7	5.4	0.34	0.39	0.43	0.47	0.54
Pd-PANI/(−)IGS	2.8	3.2	3.6	4.3	4.5	0.28	0.32	0.36	0.43	0.45

reduce any liquid sealing effect. The enhanced electrocatalytic activity of the Pd-PANI nanocomposite deposited on exfoliated graphite sheet can be attributed to (i) its ability to stabilize the high dispersion of Pd-PANI nanocomposite through the attached functional groups and (ii) its highly porous structure which facilitate ethanol molecules to diffuse within the catalyst layer easily and form larger three-phase interface [17,59,60]. Therefore, the effective enhancement of electrocatalytic properties of the Pd-PANI/(±)IGS composite arises not only due to the exfoliation process, but also because of the good dispersion of the nanocomposite and the effective lateral surface interactions between the substrate and the nanocomposite.

Table 5
Activation energy (E_a) values at different potentials for EOR on Pd/GS and Pd-PANI/GS electrode.

E (V)	E_a (kJ/mol)	
	Pd/GS	Pd-PANI/GS
−0.25	25.9	19.6
−0.2	29.9	17.5
−0.15	28.6	15.6
−0.1	26.7	14.1
−0.05	24.6	12.7

3.4.7. Activation energy studies of EOR on Pd/GS, Pd-PANI/GS, Pd-PANI/(+)IGS and Pd-PANI/(−)IGS electrodes

Electro organic reactions such as alcohol oxidation on electrode surfaces require high positive potentials under normal conditions due to their inherently poor reaction kinetics. In the presence of suitable electrocatalytic material, the surface interaction lowers the activation energy required for the reaction [61]. EOR is one such reaction which takes place at higher oxidation potentials yielding relatively low current density. An inert electrode, like for example, graphite and noble metals like Pt, Au, Ag and Pd are known to show varying extent of electrocatalytic behavior toward EOR. By immobilizing the noble metal atoms along with conductive polymer material, the electrocatalytic activity of the metal nanoparticles can be further enhanced [62,63]. The surface of the nanoparticles attached on the graphite support cannot extend all their active sites for ethanol molecules. However, in the case of Pd-PANI composite, the clusters of Pd atoms are encapsulated within the polymer matrix making more surface sites to be available for reaction with the solute molecules [26,28].

Fig. 9 shows Arrhenius plots of (A) Pd/GS and (B) Pd-PANI/GS electrodes in 0.2 M ethanol using 0.1 M NaOH respectively. Activation energy (E_a) values measured from the slopes ($-E_a/2.303R$) obtained for the plots log I *vs.* $1/T$ are shown in Table 5. The linear relationship in these plots suggests that the mechanism essentially remains the same at the temperature range of our study. Table 5 also shows that E_a value of Pd-PANI/GS is significantly lower when compared to the Pd/GS. The values of activation energy obtained in our study are significantly lower when compared to the earlier works where they range from 25 to 50 kJ/mol [27,53,64,65]. This can be accounted for (i) the anti-fouling ability of Pd-PANI during the EOR and (ii) by the enhanced EOR kinetics due to the large number of catalytically active sites present on a porous globular network of Pd-PANI as seen in the FESEM images of Fig. 1. The Pd nanoparticles are well dispersed and optimally adhering on the network of PANI which provides multiple active sites for the ethanol molecules to adsorb on the surface initially. The continuous renewal of active sites by facile desorption of reaction intermediates at higher temperatures can explain the enhanced electrocatalytic activity of Pd-PANI nanocomposite material.

Fig. 10 shows the Arrhenius plots obtained for (A) Pd-PANI/(+)IGS and (B) Pd-PANI/(−)IGS electrodes in 0.04 M ethanol + 0.1 M NaOH aqueous solution. The activation energy studies were carried out between the potential ranges −0.4 to −0.2 V *vs.* MMO at varying the temperature from 15 to 35 °C. The low activation energy values clearly suggest that the deposited nanocomposite on the exfoliated substrates enhance the electrocatalytic property toward EOR. The increased surface area by the electrochemical exfoliation and numerous defects introduced during the process on the graphite surface lead to a 3-

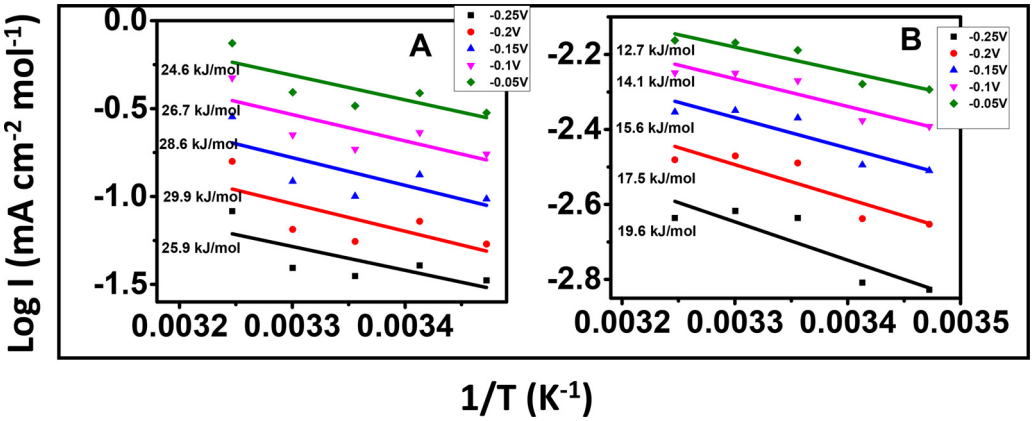

Fig. 9. Arrhenius plots at different over potentials for ethanol oxidation reaction (EOR) at (A) Pd/GS and (B) Pd-PANI/GS electrode in 0.2 M ethanol using 0.1 M NaOH respectively.

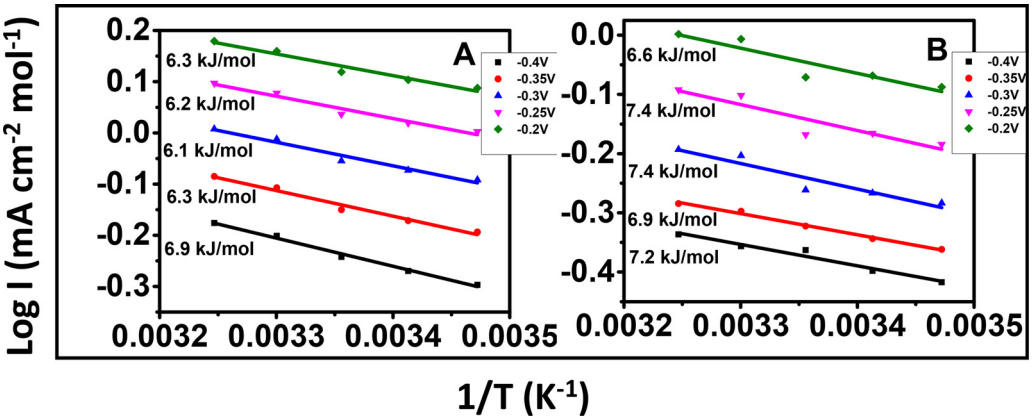

Fig. 10. Arrhenius plots at different over potential (η) values for (A) Pd-PANI/(+)IGS and (B) Pd-PANI/(−) IGS electrode in 0.04 M ethanol using 0.1 M NaOH respectively.

Table 6
Activation energy (E_a) values at different potentials for EOR on Pd-PANI/(+) IGS and Pd-PANI/(−)IGS electrodes.

E (V)	E_a (kJ/mol)	
	Pd-PANI/(+)IGS	Pd-PANI/(−)IGS
−0.4	6.9	7.2
−0.35	6.3	6.9
−0.3	6.1	7.4
−0.25	6.2	7.0
−0.2	6.3	6.6

dimensional network structure. Such a structure provides more channels for the reactants to convert into products. In addition, the formation of hydrophilic functional groups (–OH, –O– and –COOH) during the process of exfoliation enhances the interactions of ethanol molecules to the surface through hydrogen bonding with –OH group of the latter [10,25].

From Table 6, it is seen that the activation energy (E_a) values for ethanol oxidation are almost half of that for Pd-PANI/(±)IGS when compared to that of Pd-PANI/GS. This can be attributed to the microporous channels created on graphite surface after exfoliation behaving as individual nanoscale reaction centers.

These values are quite comparable with $Pt_{30}Pd_{38}Au_{32}$ on C (4 kJ/mol) reported in literature for ethanol oxidation in alkaline medium [66]. Recent reports on ethanol oxidation using different electrocatalytic materials have shown higher activation energy values of 18 kJ/mol (β-NiOOH) [50], 22 kJ/mol (Pd-PANI) [65] and 37 kJ/mol (Au-PANI) [67]. The remarkable electrocatalytic activity achieved by the nanocomposite on exfoliated substrates can be attributed to the numerous edges and corners in the polyhedral shaped nanoclusters of Pd present on the exfoliated graphite surface [68]. In addition, the conductive polymer possess 3D network with channels and pores on the electrode surface, through which the liquid fuel can easily diffuse to the catalyst sites [60,69].

4. Conclusions

Electrochemical exfoliation of flexible graphite sheets was carried out by the application of electrochemical potential in acetonitrile solvent with tetrabutylammonium tetrafluoroborate as a supporting electrolyte. The exfoliated graphite was used as an integral electrode material for immobilizing Pd nanoparticles and Pd-PANI nanocomposite by electrodeposition. The high Pd loading obtained for the substrates are due to the presence of large number of edge planes and defects created over the surface. These defects act as heterogeneous sites for the deposition of catalytic material. Similar method was adopted for depositing Pd-PANI nanocomposite on the electrodes. The large number of functional groups introduced on the flexible graphite substrate during the exfoliation process and the encapsulation of Pd nanoparticles within the PANI matrix aid in the significant lowering of the activation energy for the reaction thereby enhancing the overall electrocatalytic activity.

Acknowledgements

We are thankful to Dr. Arun Roy for his help in Raman studies. We thank Mr. Dhason and Mr. Yatheendran for their technical help in carrying SEM, STEM and EDAX, Mr. Mani for fabrication of electrode holders and Mrs. N. Vasudha for XRD studies.

Appendix A. Supplementary data

Supplementary data associated with this article can be found, in the online version, at https://doi.org/10.1016/j.apcatb.2019.03.030.

References

[1] G.R. Dieckmann, S.H. Langer, Comparisons of Ebonex® and graphite supports for platinum and nickel electrocatalysts, Electrochim. Acta 44 (1998) 437–444, https://doi.org/10.1016/S0013-4686(98)00061-9.
[2] S. Bong, Y.R. Kim, I. Kim, S. Woo, S. Uhm, J. Lee, H. Kim, Graphene supported electrocatalysts for methanol oxidation, Electrochem. Commun. 12 (2010) 129–131, https://doi.org/10.1016/j.elecom.2009.11.005.
[3] B. Fang, N.K. Chaudhari, M.-S. Kim, J.H. Kim, J.-S. Yu, Homogeneous deposition of platinum nanoparticles on carbon black for proton exchange membrane fuel cell, J. Am. Chem. Soc. 131 (2009) 15330–15338, https://doi.org/10.1021/ja905749e.
[4] I.G. David, D.E. Popa, M. Buleandra, Pencil graphite electrodes: a versatile tool in electroanalysis, J. Anal. Methods Chem. 2017 (2017), https://doi.org/10.1155/2017/1905968.
[5] G. Lu, G. Zangari, Electrodeposition of platinum on highly oriented pyrolytic graphite. Part I: Electrochemical characterization, J. Phys. Chem. B 109 (2005) 7998–8007, https://doi.org/10.1021/jp0407324.
[6] B. Zhang, D.S. Su, Probing the metal–support interaction in carbon-supported catalysts by using electron microscopy, ChemCatChem 7 (2015) 3639–3645, https://doi.org/10.1002/cctc.201500666.
[7] J.J. Liu, Advanced electron microscopy of metal–support interactions in supported metal catalysts, ChemCatChem 3 (2011) 934–948, https://doi.org/10.1002/cctc.201100090.
[8] H.N. Pham, A.E. Anderson, R.L. Johnson, T.J. Schwartz, B.J. O'Neill, P. Duan, K. Schmidt-Rohr, J.A. Dumesic, A.K. Datye, Carbon overcoating of supported metal catalysts for improved hydrothermal stability, ACS Catal. 5 (2015) 4546–4555, https://doi.org/10.1021/acscatal.5b00329.
[9] P. Ehrburger, O. Mahajan, P. Walkerjr, Carbon as a support for catalysts. I. Effect of surface heterogeneity of carbon on dispersion of platinum, J. Catal. 43 (1976) 61–67, https://doi.org/10.1016/0021-9517(76)90293-1.
[10] C. Xu, L. Cheng, P. Shen, Y. Liu, Methanol and ethanol electrooxidation on Pt and Pd supported on carbon microspheres in alkaline media, Electrochem. Commun. 9 (2007) 997–1001, https://doi.org/10.1016/j.elecom.2006.12.003.
[11] Z. Xu, C. Duong-Viet, Y. Liu, W. Baaziz, B. Li, L. Nguyen-Dinh, O. Ersen, C. Pham-Huu, Macroscopic graphite felt containing palladium catalyst for liquid-phase hydrogenation of cinnamaldehyde, Appl. Catal. B: Environ. 244 (2019) 128–139,

https://doi.org/10.1016/j.apcatb.2018.11.041.
[12] E. Pérez-Mayoral, V. Calvino-Casilda, E. Soriano, Metal-supported carbon-based materials: opportunities and challenges in the synthesis of valuable products, Catal. Sci. Technol. (2016), https://doi.org/10.1039/c5cy01437a.
[13] H. Xiong, L.L. Jewell, N.J. Coville, Shaped carbons as supports for the catalytic conversion of syngas to clean fuels, ACS Catal. (2015), https://doi.org/10.1021/acscatal.5b00090.
[14] S.H. Joo, S.J. Choi, I. Oh, J. Kwak, Z. Liu, O. Terasaki, R. Ryoo, Ordered nanoporous arrays of carbon supporting high dispersions of platinum nanoparticles, Nature 412 (2001) 169–172, https://doi.org/10.1038/35084046.
[15] N. Ostojic, R.M. Crooks, Electrocatalytic reduction of oxygen on platinum nanoparticles in the presence and absence of interactions with the electrode surface, Langmuir (2016), https://doi.org/10.1021/acs.langmuir.6b02578.
[16] I. Geukens, D.E. De Vos, Organic transformations on metal nanoparticles: Controlling activity, stability, and recyclability by support and solvent interactions, Langmuir (2013), https://doi.org/10.1021/la304639z.
[17] C.A. Frysz, D.D.L. Chung, Electrochemical behavior of flexible graphite, Carbon (N. Y.) 35 (1997) 858–860, https://doi.org/10.1016/S0008-6223(97)80175-3.
[18] W. Yuan, Y. Zhou, Y. Li, C. Li, H. Peng, J. Zhang, Z. Liu, L. Dai, G. Shi, The edge- and basal-plane-specific electrochemistry of a single-layer graphene sheet, Sci. Rep. 3 (2013) 2248, https://doi.org/10.1038/srep02248.
[19] M. Nakahara, Y. Sanada, FT-IR ATR spectroscopy of the edge surface of pyrolytic graphite and its surface/PVC interface, J. Mater. Sci. 30 (1995) 4363–4368, https://doi.org/10.1007/BF00361518.
[20] M. Mahmoodinia, P.-O. Åstrand, D. Chen, Influence of carbon support on electronic structure and catalytic activity of Pt catalysts: binding to the CO molecule, J. Phys. Chem. C 120 (2016) 12452–12462, https://doi.org/10.1021/acs.jpcc.6b02001.
[21] C. Zhai, M. Sun, L. Zeng, M. Xue, J. Pan, Y. Du, M. Zhu, Construction of Pt/graphitic C_3N_4/MoS_2 heterostructures on photo-enhanced electrocatalytic oxidation of small organic molecules, Appl. Catal. B: Environ. 243 (2019) 283–293, https://doi.org/10.1016/j.apcatb.2018.10.047.
[22] I.S. Pieta, A. Rathi, P. Pieta, R. Nowakowski, M. Hołdynski, M. Pisarek, A. Kaminska, M.B. Gawande, R. Zboril, Electrocatalytic methanol oxidation over Cu, Ni and bimetallic Cu–Ni nanoparticles supported on graphitic carbon nitride, Appl. Catal. B: Environ. 244 (2019) 272–283, https://doi.org/10.1016/j.apcatb.2018.10.072.
[23] T. Öznülüer, Ü. Demir, H. Öztürk Doğan, Fabrication of underpotentially deposited Cu monolayer/electrochemically reduced graphene oxide layered nanocomposites for enhanced ethanol electro-oxidation, Appl. Catal. B: Environ. 235 (2018) 56–65, https://doi.org/10.1016/j.apcatb.2018.04.065.
[24] E. Antolini, Catalysts for direct ethanol fuel cells, J. Power Sources 170 (2007) 1–12, https://doi.org/10.1016/j.jpowsour.2007.04.009.
[25] E. Antolini, E.R. Gonzalez, Alkaline direct alcohol fuel cells, J. Power Sources 195 (2010) 3431–3450, https://doi.org/10.1016/j.jpowsour.2009.11.145.
[26] R.K. Pandey, V. Lakshminarayanan, Electro-oxidation of formic acid, methanol, and ethanol on electrodeposited Pd-polyaniline nanofiber films in acidic and alkaline medium, J. Phys. Chem. C 113 (2009) 21596–21603, https://doi.org/10.1021/jp908239m.
[27] R.K. Pandey, V. Lakshminarayanan, Ethanol electrocatalysis on gold and conducting polymer nanocomposites: A study of the kinetic parameters, Appl. Catal. B: Environ. 125 (2012) 271–281, https://doi.org/10.1016/j.apcatb.2012.06.002.
[28] S. Ghosh, A.-L. Teillout, D. Floresyona, P. de Oliveira, A. Hagège, H. Remita, Conducting polymer-supported palladium nanoplates for applications in direct alcohol oxidation, Int. J. Hydrogen Energy 40 (2015) 4951–4959, https://doi.org/10.1016/j.ijhydene.2015.01.101.
[29] R. Santhanam, M. Noel, Effect of solvents on the intercalation/de-intercalation behaviour of monovalent ionic species from non-aqueous solvents on polypropylene-graphite composite electrode, J. Power Sources 66 (1997) 47–54, https://doi.org/10.1016/S0378-7753(96)02472-X.
[30] B.H. Ka, S.M. Oh, Electrochemical activation of expanded graphite electrode for electrochemical capacitor, J. Electrochem. Soc. 155 (2008) A685, https://doi.org/10.1149/1.2953525.
[31] R. Santhanam, M. Noel, Electrochemical intercalation of ionic species of tetrabutylammonium perchlorate on graphite electrodes. A potential dual-intercalation battery system, J. Power Sources 56 (1995) 101–105, https://doi.org/10.1016/0378-7753(95)80016-A.
[32] M. Noel, R. Santhanam, Electrochemistry of graphite intercalation compounds, J. Power Sources 72 (1998) 53–65, https://doi.org/10.1016/S0378-7753(97)02675-X.
[33] P. Yu, S.E. Lowe, G.P. Simon, Y.L. Zhong, Electrochemical exfoliation of graphite and production of functional graphene, Curr. Opin. Colloid Interface Sci. 20 (2015) 329–338, https://doi.org/10.1016/j.cocis.2015.10.007.
[34] A. Ambrosi, C.K. Chua, A. Bonanni, M. Pumera, Electrochemistry of graphene and related materials, Chem. Rev. 114 (2014) 7150–7188, https://doi.org/10.1021/cr500023c.
[35] M. Milica, Z. Branimir, S. Jasmina, L. Tomislav, N. Branimir, Electrochemical polymerization of aniline, Electropolymerization, InTech, 2011, pp. 77–96, https://doi.org/10.5772/28293.
[36] T. Sri Devi Kumari, A.J.J. Jebaraj, T.A. Raj, D. Jeyakumar, T.P. Kumar, A kish graphitic lithium-insertion anode material obtained from non-biodegradable plastic waste, Energy 95 (2016) 483–493, https://doi.org/10.1016/j.energy.2015.11.069.
[37] P. Ramesh, S. Sampath, Selective determination of uric acid in presence of ascorbic acid and dopamine at neutral pH using exfoliated graphite electrodes, Electroanalysis 16 (2004) 866–869, https://doi.org/10.1002/elan.200302890.
[38] M. Zhou, J. Tang, Q. Cheng, G. Xu, P. Cui, L.C. Qin, Few-layer graphene obtained by electrochemical exfoliation of graphite cathode, Chem. Phys. Lett. 572 (2013) 61–65, https://doi.org/10.1016/j.cplett.2013.04.013.
[39] A. Milev, M. Wilson, G.S.K. Kannangara, N. Tran, X-ray diffraction line profile analysis of nanocrystalline graphite, Mater. Chem. Phys. 111 (2008) 346–350, https://doi.org/10.1016/j.matchemphys.2008.04.024.
[40] J. Yu, T. Fujita, A. Inoue, T. Sakurai, M. Chen, Electrochemical synthesis of palladium nanostructures with controllable morphology, Nanotechnology 21 (2010) 085601, https://doi.org/10.1088/0957-4484/21/8/085601.
[41] Y. Li, G. Lu, X. Wu, G. Shi, Electrochemical fabrication of two-dimensional palladium nanostructures as substrates for surface enhanced raman scattering, J. Phys. Chem. B 110 (2006) 24585–24592, https://doi.org/10.1021/jp0638787.
[42] Z.P. Sun, X.G. Zhang, Y.Y. Liang, H.L. Li, A facile approach towards sulfonate functionalization of multi-walled carbon nanotubes as Pd catalyst support for ethylene glycol electro-oxidation, J. Power Sources 191 (2009) 366–370, https://doi.org/10.1016/j.jpowsour.2009.01.093.
[43] L. Xiao, L. Zhuang, Y. Liu, J. Lu, Activating Pd by morphology tailoring for oxygen reduction, J. Am. Chem. Soc. 131 (2009) 602–608, https://doi.org/10.1021/ja8063765.
[44] W. Pan, X. Zhang, H. Ma, J. Zhang, Electrochemical synthesis, voltammetric behavior, and electrocatalytic activity of Pd nanoparticles, J. Phys. Chem. C 112 (2008) 2456–2461, https://doi.org/10.1021/jp710092z.
[45] M. Shibata, S. Motoo, Electrocatalysis by ad-atoms. Part I. Enhancement of the oxidation of methanol on platinum and palladium by gold ad-atoms, J. Electroanal. Chem. Interfacial Electrochem. 209 (1986) 151–158, https://doi.org/10.1016/0022-0728(86)80193-0.
[46] Z.X. Liang, T.S. Zhao, J.B. Xu, L.D. Zhu, Mechanism study of the ethanol oxidation reaction on palladium in alkaline media, Electrochim. Acta 54 (2009) 2203–2208, https://doi.org/10.1016/j.electacta.2008.10.034.
[47] Y. Wang, S. Zou, W.-B. Cai, Recent advances on electro-oxidation of ethanol on Pt- and Pd-based catalysts: from reaction mechanisms to catalytic materials, Catalysts 5 (2015) 1507–1534, https://doi.org/10.3390/catal5031507.
[48] C. Lamy, E.M. Belgsir, J.M. Léger, Electrocatalytic oxidation of aliphatic alcohols: Application to the direct alcohol fuel cell (DAFC), J. Appl. Electrochem. 31 (2001) 799–809, https://doi.org/10.1023/A:1017587310150.
[49] Q. Kong, W. Feng, X. Zhu, J. Zhang, C. Sun, Fabrication, characterization and electrochemical properties of porous palladium bulk samples with high porosity and hierarchical pore structure, Chin. J. Catal. 38 (2017) 1038–1044, https://doi.org/10.1016/S1872-2067(17)62780-3.
[50] A.F.B. Barbosa, V.L. Oliveira, J. van Drunen, G. Tremiliosi-Filho, Ethanol electrooxidation reaction using a polycrystalline nickel electrode in alkaline media: Temperature influence and reaction mechanism, J. Electroanal. Chem. 746 (2015) 31–38, https://doi.org/10.1016/j.jelechem.2015.03.024.
[51] D. Chu, Methanol electro-oxidation on unsupported Pt–Ru alloys at different temperatures, J. Electrochem. Soc. 143 (1996) 1685, https://doi.org/10.1149/1.1836700.
[52] A.V. Tripković, K.D. Popović, J.D. Lović, The influence of the oxygen-containing species on the electrooxidation of the C1–C4 alcohols at some platinum single crystal surfaces in alkaline solution, Electrochim. Acta 46 (2001) 3163–3173, https://doi.org/10.1016/S0013-4686(01)00608-9.
[53] L. Ma, D. Chu, R. Chen, Comparison of ethanol electro-oxidation on Pt/C and Pd/C catalysts in alkaline media, Int. J. Hydrogen Energy 37 (2012) 11185–11194, https://doi.org/10.1016/j.ijhydene.2012.04.132.
[54] H. Wang, Z. Jusys, R.J. Behm, Ethanol electrooxidation on a carbon-supported Pt catalyst: reaction kinetics and product yields, J. Phys. Chem. B 108 (2004) 19413–19424, https://doi.org/10.1021/jp046561k.
[55] R.S. Sai Siddhardha, M. Anupam Kumar, V. Lakshminarayanan, S.S. Ramamurthy, Anti-fouling response of gold-carbon nanotubes composite for enhanced ethanol electrooxidation, J. Power Sources 271 (2014) 305–311, https://doi.org/10.1016/j.jpowsour.2014.08.023.
[56] F. Kaedi, Z. Yavari, M. Noroozifar, H. Saravani, Promoted electrocatalytic ability of the Pd on doped Pt in NiO–MgO solid solution toward methanol and ethanol oxidation, J. Electroanal. Chem. 827 (2018) 204–212, https://doi.org/10.1016/j.jelechem.2018.09.025.
[57] E.M. Gacutan, M.I. Climaco, G.J. Telan, F. Malijan, H.Y. Hsu, J. Garcia, H. Fulo, B.J. Tongol, Nanostructured carbon-supported Pd electrocatalysts for ethanol oxidation: Synthesis and characterization, Adv. Nat. Sci. Nanosci. Nanotechnol. 3 (2012), https://doi.org/10.1088/2043-6262/3/4/045016.
[58] Y.X. Huang, J.F. Xie, X. Zhang, L. Xiong, H.Q. Yu, Reduced graphene oxide supported palladium nanoparticles via photoassisted citrate reduction for enhanced electrocatalytic activities, ACS Appl. Mater. Interfaces 6 (2014) 15795–15801, https://doi.org/10.1021/am504664r.
[59] Y.C. Liu, X.P. Qiu, Y.Q. Huang, W.T. Zhu, Methanol electro-oxidation on mesocarbon microbead supported Pt catalysts, Carbon (N. Y.) 40 (2002) 2375–2380, https://doi.org/10.1016/S0008-6223(02)00115-X.
[60] F. Xie, Z. Tian, H. Meng, P.K. Shen, Increasing the three-phase boundary by a novel three-dimensional electrode, J. Power Sources 141 (2005) 211–215, https://doi.org/10.1016/j.jpowsour.2004.10.002.
[61] D. Pletcher, R. Greff, R. Peat, L.M. Peter, J. Robinson, Instrumental Methods in Electrochemistry, Horwood Publishers, 2011 https://www.sciencedirect.com/science/book/9781898563808.
[62] C.T. Hable, M.S. Wrighton, Electrocatalytic oxidation of methanol by assemblies of platinum/tin catalyst particles in a conducting polyaniline matrix, Langmuir 7 (1991) 1305–1309, https://doi.org/10.1021/la00055a001.
[63] P.O. Esteban, J.M. Leger, C. Lamy, E. Genies, Electrocatalytic oxidation of methanol on platinum dispersed in polyaniline conducting polymers, J. Appl. Electrochem. 19 (1989) 462–464, https://doi.org/10.1007/BF01015254.
[64] S.T. Nguyen, H.M. Law, H.T. Nguyen, N. Kristian, S. Wang, S.H. Chan, X. Wang,

Enhancement effect of Ag for Pd/C towards the ethanol electro-oxidation in alkaline media, Appl. Catal. B: Environ. 91 (2009) 507–515, https://doi.org/10.1016/j.apcatb.2009.06.021.
[65] R.K. Pandey, S. Patnaik, V. Lakshminarayanan, Thin film of palladium nanodendrites supported on graphite electrode for catalyzing the oxidation of small organic molecules, Catal. Lett. 144 (2014) 965–970, https://doi.org/10.1007/s10562-014-1219-3.
[66] J. Datta, A. Dutta, S. Mukherjee, The beneficial role of the cometals Pd and Au in the carbon-supported PtPdAu catalyst toward promoting ethanol oxidation kinetics in alkaline fuel cells: Temperature effect and reaction mechanism, J. Phys. Chem. C 115 (2011) 15324–15334, https://doi.org/10.1021/jp200318m.
[67] R.K. Pandey, V. Lakshminarayanan, Ethanol electrocatalysis on gold and conducting polymer nanocomposites: A study of the kinetic parameters, Appl. Catal. B: Environ. 125 (2012) 271–281, https://doi.org/10.1016/j.apcatb.2012.06.002.
[68] S.C.S. Lai, M.T.M. Koper, The influence of surface structure on selectivity in the ethanol electro-oxidation reaction on platinum, J. Phys. Chem. Lett. 1 (2010) 1122–1125, https://doi.org/10.1021/jz100272f.
[69] M. Wang, X. Song, Q. Yang, H. Hua, S. Dai, C. Hu, D. Wei, Pt nanoparticles supported on graphene three-dimensional network structure for effective methanol and ethanol oxidation, J. Power Sources 273 (2015) 624–630, https://doi.org/10.1016/j.jpowsour.2014.09.117.